

FFI RAPPORT

NUMERICAL SIMULATION OF LIGHT ARMOUR PIERCING AMMUNITION AGAINST STEEL

TELAND Jan Arild

FFI/RAPPORT-2005/00126

FFI-V/870/130

Approved
Kjeller 13. January 2004

Bjarne Haugstad
Director of Research

**NUMERICAL SIMULATION OF LIGHT
ARMOUR PIERCING AMMUNITION AGAINST
STEEL**

TELAND Jan Arild

FFI/RAPPORT-2005/00126

FORSVARETS FORSKNINGSINSTITUTT
Norwegian Defence Research Establishment
P O Box 25, NO-2027 Kjeller, Norway

FORSVARETS FORSKNINGSINSTITUTT (FFI)
Norwegian Defence Research Establishment

UNCLASSIFIED

P O BOX 25
 NO-2027 KJELLER, NORWAY
REPORT DOCUMENTATION PAGE

SECURITY CLASSIFICATION OF THIS PAGE
 (when data entered)

1) PUBL/REPORT NUMBER FFI/RAPPORT-2005/00126	2) SECURITY CLASSIFICATION UNCLASSIFIED	3) NUMBER OF PAGES 31
1a) PROJECT REFERENCE FFI-V/870/130	2a) DECLASSIFICATION/DOWNGRADING SCHEDULE -	
4) TITLE NUMERICAL SIMULATION OF LIGHT ARMOUR PIERCING AMMUNITION AGAINST STEEL		
5) NAMES OF AUTHOR(S) IN FULL (surname first) TELAND Jan Arild		
6) DISTRIBUTION STATEMENT Approved for public release. Distribution unlimited. (Offentlig tilgjengelig)		
7) INDEXING TERMS IN ENGLISH:		
a) <u>Penetration</u>		IN NORWEGIAN:
b) <u>Steel</u>		a) <u>Penetrasjon</u>
c) <u>Ceramics</u>		b) <u>Stål</u>
d) <u>Kevlar-Epoxy</u>		c) <u>Keramikk</u>
e) <u>Numerical simulation</u>		d) <u>Kevlar-Epoxy</u>
		e) <u>Numerisk simulering</u>
THESAURUS REFERENCE:		
8) ABSTRACT <p>Numerical simulations using the hydrocode Autodyn of two different armour piercing projectiles are performed against steel and ceramic targets. The results are compared with some experimental data available. A major problem was that no exact material data for the projectiles and targets are available. Only values for the Vicker's hardness of the projectile cores are given, which can not be directly converted to material parameters required by Autodyn. Before proceeding with simulations of more complex target configurations, it would be worthwhile to establish more reliable material data for the projectiles.</p>		
9) DATE 13. januar 2004	AUTHORIZED BY This page only Bjarne Haugstad	POSITION Director of Research

ISBN 82-464-0977-8

UNCLASSIFIED

SECURITY CLASSIFICATION OF THIS PAGE
 (when data entered)

CONTENTS

	Page
1 INTRODUCTION	7
2 PROJECTILES	7
3 EXPERIMENTS	8
4 HYDROCODE MODEL	8
4.1 Bofors FFV	9
4.2 Fabrique National P80	9
4.3 Target plate	10
5 MATERIAL MODELS	10
5.1 Steel	10
5.1.1 Johnson-Cook yield model	10
5.1.2 Vicker's hardness	10
5.2 Conversion of data	11
5.3 Tungsten Carbide	12
5.4 Lead	12
5.5 Brass	12
5.6 Alumina	12
5.7 Kevlar-Epoxy	12
6 ANALYTICAL PERFORATION MODEL	13
6.1 Cavity expansion theory	13
6.2 Boundary effects	14
7 JACKET STRIPPING	14
8 COMPARISON WITH EXPERIMENTS	15
9 COMPARISON WITH TNO-EXPERIENCES	16
10 CONCLUSION	16
References	17
A CONVERSION CHART FOR VICKER'S HARDNESS TO YIELD STRENGTH	18
B MATERIAL MODELS	18

NUMERICAL SIMULATION OF LIGHT ARMOUR PIERCING AMMUNITION AGAINST STEEL

1 INTRODUCTION

In Project 870 one of the goals is to be able to simulate penetration of various types of projectiles into (light) armour materials. However, before moving on to study exotic materials with partly unknown material parameters, it is important to check that the hydrocode is able to give correct results for penetration into more common materials.

In this report we examine the penetration of two particular AP projectiles into various materials, in particular steel. The reason is that some experimental data is available for these projectiles. Most of the work will be numerical simulations but we also compare with experiments and analytical theory where available.

2 PROJECTILES

We will especially study two very common types of ammunition, namely the 7.62 x 51 FFV Bofors AB projectile with a tungsten carbide core and the 7.62 x 51 AP Fabrique National projectile with a hard steel core. These projectiles are shown in Figure 2.1.



Figure 2.1: The projectiles and cores that are studied in this report.

We have so far been unable to dissect and examine the contents of the FN projectiles, but it is widely known (1) that NM61 projectiles from Raufoss, for which we have projectiles

available, are made after (almost) the same standard. Further, 7.62 x 51 Carl Gustav (CG) with a tungsten carbide core are the same as 7.62 x 51 FFV from Bofors.

3 EXPERIMENTS

As mentioned, several experiments with these projectiles have been carried out by Horsfall et.al. (2). The aim of their experiments was to compare the performance of four different types of light-armour piercing ammunition against various targets. As far as we are aware, this is one of very few, available scientific papers with data for commercially available projectiles. It was therefore of interest for us to see whether we would be able to reproduce these results using numerical simulations. Our idea was that, before embarking on performing simulations of complex situations involving exotic materials, it was necessary to be able to obtain relatively accurate results for this case.

The tests are described in (2), although, unfortunately, few details were given about the set-up of the tests themselves. However, it appears that the ballistic limit V_{50} was determined, sometimes together with the V_0 ballistic limit, by performing a linear regression analysis on a pendulum displacement versus impact velocity data.

Three types of targets were used:

- Mild steel: 300 mm x 300 mm x 12 mm, Hardness HV 135
- Hard steel: 250 mm x 250 mm x 9.4 mm, Hardness HV 464
- Ceramic faced composite: 8.0 mm 95% alumina ceramic bonded to an aramid composite backing of thickness 6.5 mm.

4 HYDROCODE MODEL

There were no indications of yawed or oblique impact in the experiments. It should therefore be sufficient to model the situation in 2D since the projectile was symmetric around the axis. For numerical simulations we therefore used the hydrocode Autodyn-2D v4.3 (3).

Autodyn has several different processors for modelling, including Lagrange, Euler and SPH. The Lagrange processor is typically suitable for objects that have some strength and an initial shape. The Euler processor is typically for a material with no pre-defined shape (like fluids, gases), but it is also often used for objects that will be strongly deformed (like a target in a penetration experiment). SPH is a meshless technique usually used for brittle objects to model cracks etc properly.

In our case the projectile core was known to remain relatively intact, and it was therefore natural to model it using Lagrange. This made it very convenient to model the complete projectile using different Lagrangian subgrids.

As for the target, either of the processors would be possible, but Euler would have been very inconvenient. For the Lagrangian projectile to interact with an Euler target, it is necessary to

define a set of polygons on the surface of the Lagrangian subgrid. This polygon boundary then deals with the interaction. For a rigid projectile this presents no problem, but in our case the jacket was known to be stripped off, which would mean that new polygons would have to be defined manually several times during the penetration process. This is of course very inconvenient when one is going to perform many simulations, as in our case.

For a ductile material such as steel, Lagrange is known to be better suited than SPH. The target plates were therefore modelled using Lagrange as well.

A problem with modelling the target in Lagrange is that several cells may become very distorted throughout the penetration process, resulting in very “thin” cells and consequently very small timesteps (and long simulation times). Or, even worse, mesh entanglement and an aborted simulation. The conventional way to deal with this is to introduce so-called numerical erosion where severely distorted cells are removed from the calculation. Obviously, it is then necessary to define a criterion for this to happen. Different strain criteria are available in Autodyn for this purpose. However, one has to be careful doing this since numerical erosion is not a physical parameter. Putting a too low value will result in cells being eroded too early (and consequently a too soft material), whereas a too strict criterion will not solve the original problem of mesh entanglement.

4.1 Bofors FFV

The Bofors projectile was modelled using a total of seven Lagrangian subgrids (two for the core, two for the aluminium and three for the brass jacket). It is shown in Figure 3.1. The subgrids for the different materials were not joined together, but interacted with each other using the interaction mechanism in Autodyn

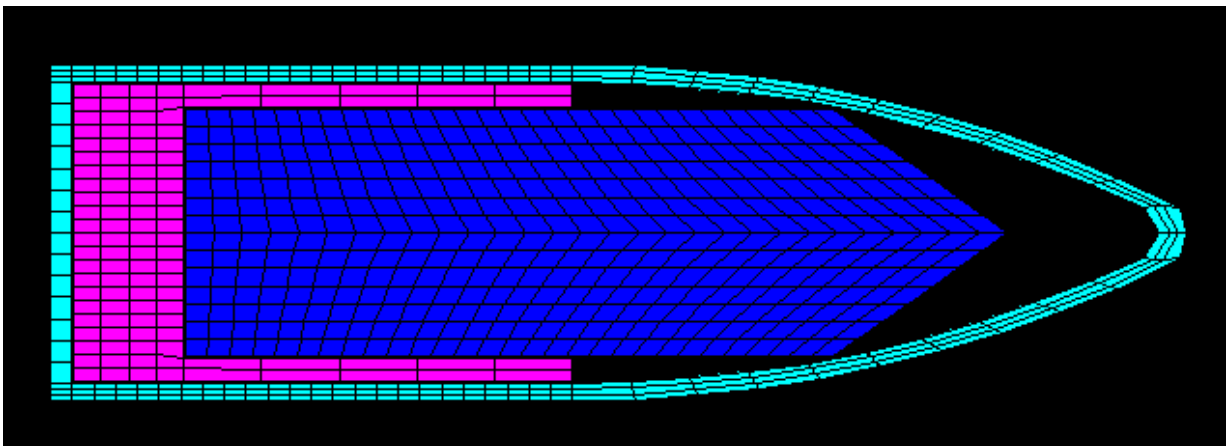


Figure 3.1: 7.62 x 51 FFV Bofors projectile.

4.2 Fabrique National P80

The P80 projectile, shown in Figure 3.2 was modelled using a total of five Lagrangian subgrids (two for the core and three for the lead and brass part). The core was not joined to the outer parts, but interacted with the interaction option. The lead and brass was for simplicity put in the same subgrid.

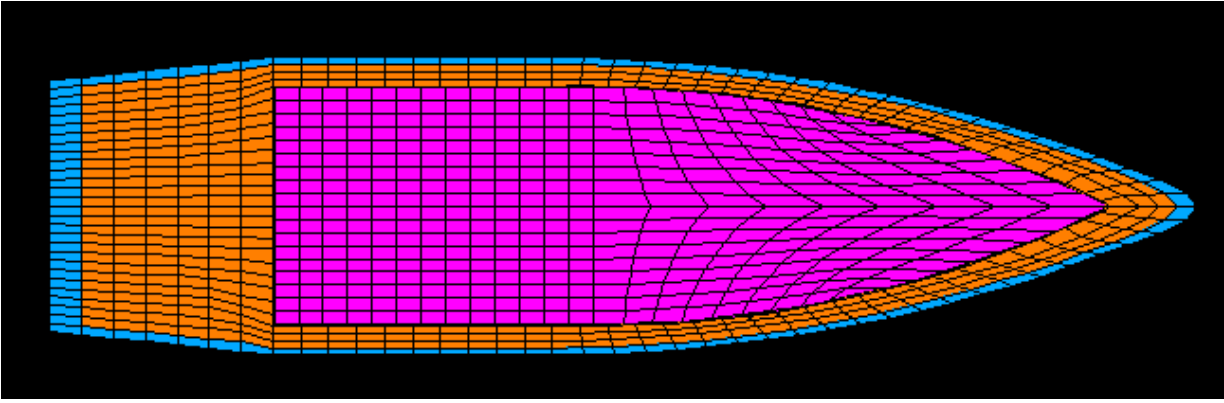


Figure 3.2: 7.62 x 51 AP Fabrique National

4.3 Target plate

The target plates were modelled in Lagrange and was made up of 0.4 mm x 0.4 mm cells in the penetration region. A coarser mesh was used in the region further out, which would not affect the main result.

5 MATERIAL MODELS

In order to compare with the experiments in (2), it is necessary that the material models used give a close description of the actual materials. Unfortunately, when limited data is available, this is easier said than done. According to Horsfall the Vicker's Hardness for the Fabrique National steel core was 870, whereas for the Bofors tungsten carbide it was 1450.

5.1 Steel

We require a steel model both for the core of the 7.62 x 51 AP FN projectile as well as the mild and hard steel target. Steel is usually considered to be a simple material to obtain data for. In a hydrocode simulation, steel is usually described by elastic parameters and a yield strength. The yield strength depends can depend on various other variables, like plastic strain and the strain rate.

5.1.1 Johnson-Cook yield model

In Autodyn it is often described using the Johnson-Cook model. The relationship between yield strength, plastic strain, strain rate and temperature is then given as follows:

$$Y = (A + B\varepsilon_p^n)(1 + C \ln \dot{\varepsilon}_p)(1 - T_H^m)$$

where A, B, C, n and m are parameters determining the material.

5.1.2 Vicker's hardness

As mentioned already, in the experiments two types of steel have been used, one mild and one hard. Unfortunately, only the Vicker's hardness for the steel types are given, whereas as we see the Johnson-Cook model in Autodyn requires several more parameters as input.

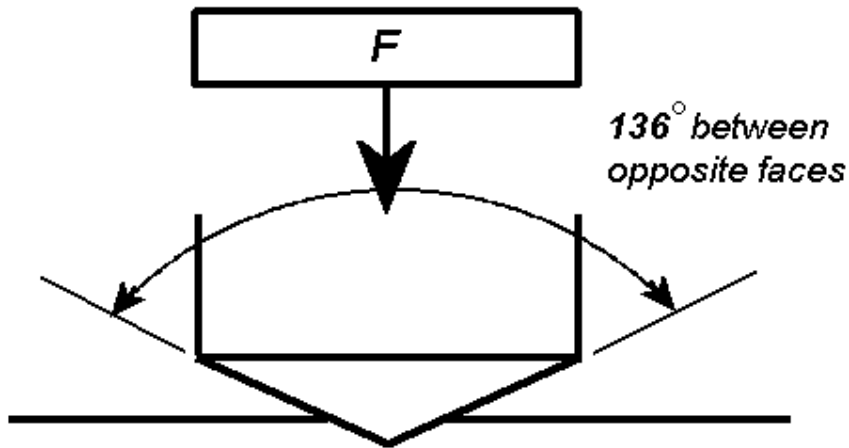


Figure 5.1: Vicker's hardness test

The Vicker's Hardness is calculated from the size of an impression produced under a quasi-static load by a pyramid-shaped diamond indenter. The indenter employed in the Vickers test is a square-based pyramid whose opposite sides meet at the apex at an angle of 136 degrees, as illustrated in Figure 5.1. The diamond is pressed into the surface of the material at loads ranging up to approximately 120 kilograms-force, and the size of the impression (usually no more than 0.5 mm) is measured with the aid of a calibrated microscope. The Vickers number (HV) is then calculated using the following formula:

$$HV = 1.854 \frac{F}{d^2}$$

with F being the applied load (measured in kilograms-force) and D^2 the area of indentation (measured in square millimeters). The applied load is usually specified when HV is cited (although this was not the case here).

Since the indentation is very small, no strain hardening is achieved during the measurement process (4). A Vicker's hardness test should then correspond to a situation with no strain rate, strain hardening or temperature effects.

To complicate matters further, there is no one-to-one correspondence between Vicker's hardness and yield strength. It depends on the applied load which was not specified. To calculate the yield strength we first converted to Brinell hardness according to (5) and then to yield strength using the same table. The conversion chart is reproduced in Appendix A.

5.2 Conversion of data

In Table 5.1 we show the given value for the Vicker's hardness of the relevant steels in (2) as well as the yield strength found by using the conversion method outlined above.

As we see, for the core of the 7.62 x 51 AP FN projectile, we obtained a yield stress of around 2.35 GPa. This is a very high value and various references (6) indicate that such a hard steel might not even exist. Later in the report this will be discussed further and we will examine the consequences of assuming a lower yield strength for the projectile.

Table 5.1: Vicker's hardness and estimated yield strength for the various steel materials.

Steel type	Vicker's hardness (HV)	Calculated yield strength
Core 7.62 x 51 AP FN	870	2350 MPa
Mild steel target	135	290 MPa
Hard steel target	464	1143 MPa

Further, it is then clear that only an estimate for the value of A is obtained from the Vicker's Hardness test. No data is available for B, C, n or m, which describe the strain hardening and strain rate sensitivity of the material. In order to get estimates for these parameters, we have used the same parameters as for the 4340 steel model in the Autodyn material library. It is clear that this is a very crude approximation, assuming implicitly that all steel types have the same strain hardening and strain rate dependence. Further, this assumption might be especially inaccurate for materials that have already been "pre-hardened" like the core of the FN projectile (the actual physics is unknown to us at the moment).

The other steel parameters have not been changed, which means that the elastic moduli and the strain rate dependence is similar for all the steel models. However, this should not be too important since elastic parameters have very little influence on the penetration process.

5.3 Tungsten Carbide

The Tungsten-Carbide model was developed at FFI (7). It uses a linear EOS together with a Mohr-Coulomb yield model and a user-defined failure model.

All material data are given in Appendix A.

5.4 Lead

For the lead jacket of the projectile we used a material model based on the lead model in the Autodyn material library. It uses the shock equation of state. In addition we added a yield limit from (8) and a numerical erosion criterion of 2.5.

5.5 Brass

For the brass we used a material model based on the brass model in the Autodyn material library. It uses the shock equation of state. In addition we added a yield limit from (8) and a numerical erosion criterion of 2.5.

5.6 Alumina

For alumina we used the model for 99.5% alumina located in the Autodyn material library (9). It uses a linear EOS and the Johnson-Holmquist strength and failure model.

5.7 Kevlar-Epoxy

For Kevlar-Epoxy we used the relatively new model developed at EMI (10). This model uses an orthotropic EOS, an elastic strength model and a tensile strain failure criterion.

6 ANALYTICAL PERFORATION MODEL

We will also compare the experimental and numerical results with an analytical perforation model. A model which is based on cavity expansion theory (CET) has been developed at FFI. It uses the FFI-extended penetration model based on CET for rigid projectiles and includes the FFI-made theory on boundary effects both from the edge and the rear end (11).

The projectile is assumed to be rigid throughout the penetration process which means that the results are really only valid for the projectile core.

6.1 Cavity expansion theory

Cavity expansion theory (CET) is often used to model penetration of rigid projectiles. In this theory the force on a penetrating projectile is estimated from the stress required to expand a cavity in the target material at a given velocity.

The first step is therefore to find a relationship between the radial stress σ_r and expansion velocity u of a cavity. This will depend on the material model, but for simple models an exact solution is possible. In an infinite medium, the radial stress can often be written on the following form:

$$\sigma_r(u) = A + Bu + Cu^2 \quad (6.1)$$

The constants A , B and C will depend on the applied target material model. For more complex material models, the CET equations can not be solved analytically and a numerical solution is necessary. However, it turns out that Equation (6.1) is usually still a very good approximation. The constants A , B and C can then be found by curve fitting to the numerical solution.

The next step is to use Equation (6.1) to estimate the stress σ_n^p on a projectile penetrating the same material. The following relationship seems to be generally accepted:

$$\sigma_n^p(v) = \sigma_r(\vec{v} \cdot \vec{n}) = A + B(\vec{v} \cdot \vec{n}) + C(\vec{v} \cdot \vec{n})^2 \quad (6.2)$$

where \vec{n} is the normal vector of the projectile surface. Analytically, a total force F can now be found by integrating the stresses over the projectile surface. Often the constant B can be set to zero and an expression on the following form can be obtained:

$$F = \alpha + \beta v^2$$

Since the projectile is assumed rigid, Newton's 2nd law can now be applied to determine the complete penetration process. In the implementation in (12) the force is calculated at every time step and the acceleration determined. Currently, the model is only implemented for ogival nose projectiles, i.e. can not be used for the FFV-projectile.

It must be noted that although CET in itself can be an exact theory, the application to penetration is just an estimate. There is a lot of empirical evidence that the approach works

well for impact on relatively soft material, though. However, possible problems with applying CET to penetration are further discussed in (13).

6.2 Boundary effects

The equation above does not account for boundary effects. Such effects can be taken into consideration by multiplying the force with a correction factor:

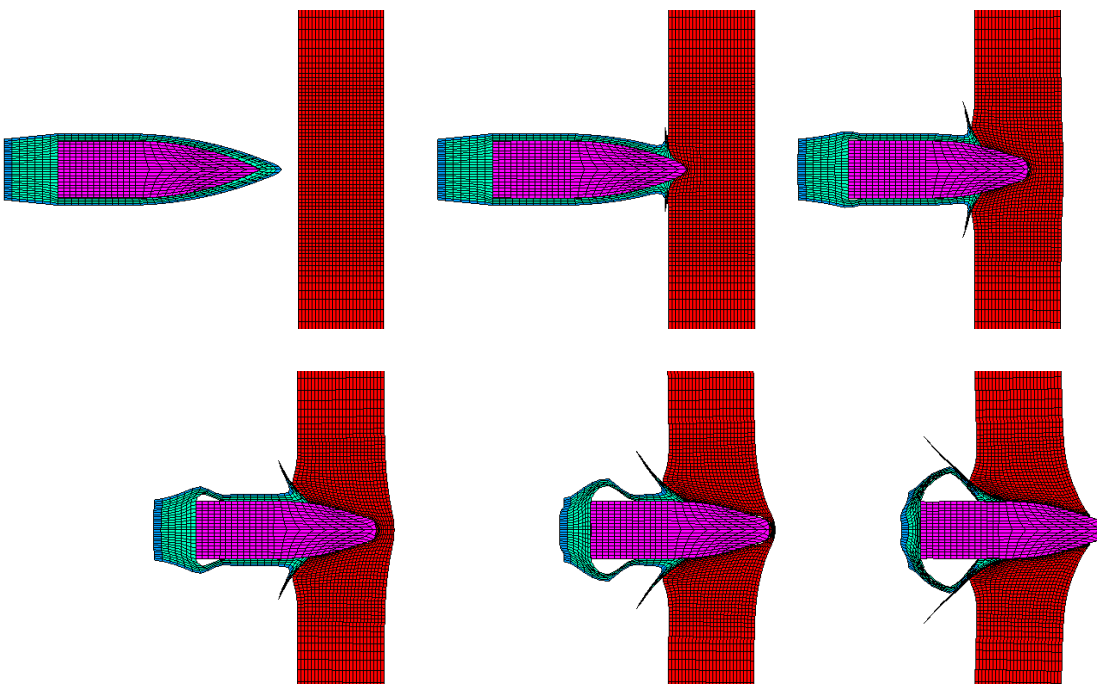
$$F \rightarrow \alpha(d)F$$

where the decay function depends on the distance to the boundary. The definition of distance to the boundary is ambiguous, as described in (14), but for perforation problems it will depend on distance to the rear side of the target and current penetration depth.

In some cases Newton's 2nd law can be solved even for this case and an analytical expression for penetration depth or ballistic limit can be found. This is discussed in detail for concrete in (11). Here we will use the tool described in (12) to calculate the penetration process. For complete details the reader is referred to this reference. We have used option 4 for boundary effects, which means that the smallest orthogonal distance to the boundary is used.

7 JACKET STRIPPING

The experiments have shown that the jacket will be stripped off the projectile core during the penetration process. This effect is seen in Figur 7.1 to be well captured by the numerical simulations. Only a few remnants of the jacket remains after the projectile has passed through the plate, which is in good agreement with experimental observations. The qualitative results therefore seem to be okay.



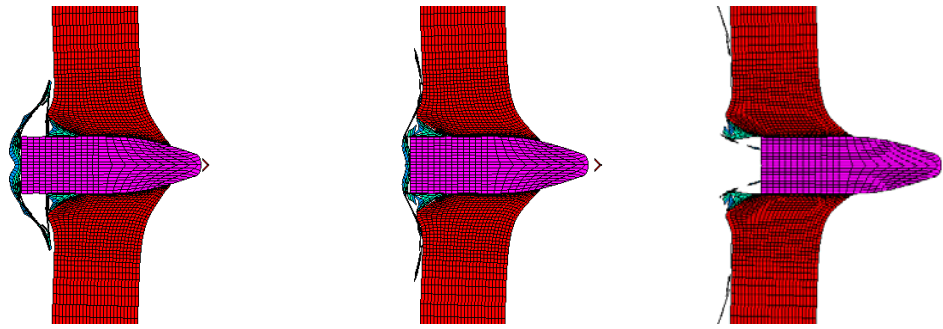


Figure 7.1: P80 projectile impact on hard steel target. Impact velocity 765 m/s. It is clearly seen how the jacket is stripped off the projectile core.

8 COMPARISON WITH EXPERIMENTS

In the numerical simulations, we modelled the projectile both with and without a jacket to see what possible influence this would have on the results.

In all cases the jacket turned out to separate from the projectile early in the penetration process. The results for ballistic limit are given in Table 1.

Table 7.1: Experimental and numerical ballistic velocities

Situation	Experiment	Simulation (core)	Simulation	Analytical
P80 Mild steel	590	564	530	577
P80 Hard steel	765	740	742	717
FFV Mild steel	487	480	490	
FFV Hard steel	502	595	600	
P80 Ceramics + Kevlar	884		370	
FFV Ceramics + Kevlar	744		320	

The agreement is seen to be reasonably good for the simulations against steel, especially considering the large uncertainty in the material data both for the projectile and the targets. However, the ceramics and Kevlar results do not agree well at all. Because of the large uncertainty in the material parameters of the materials in the actual experiments, there can be several explanations for this.

A cause of concern is, as mentioned before, that the P80 projectile core might have been given a too high yield limit. It is clear from the results that the ballistic limit is slightly lower than in the experiments, which supports this theory. Given the large uncertainty in the material

parameters, it would be reasonable to calibrate the projectile core yield limit so that the experimental ballistic limit is found.

With the current high yield limit, the projectile perforates the target without hardly any visible deformation of the projectile core. By lowering the yield limit to around $Y=2.1$ GPa, we reproduce the experimental result exactly for hard steel target. Using 1.7 GPa gives a visible deformation of the projectile, which is then unable to perforate the target at an impact velocity of 765 m/s.

However, a yield limit of 1.7 GPa gives an exit velocity of 297 m/s for an impact velocity of 590 m/s for the mild steel target. Lowering the yield limit further to 1.0 GPa still gives an exit velocity of 232 m/s. Clearly it will be impossible to make those two results agree with each other without also modifying the yield limit (properties) of both target steels. By tampering with the various steel models we will clearly be able to reproduce any experimental result, though. Again it is unfortunate that we only have material data for the Vicker's hardness and no other physical parameters.

9 COMPARISON WITH TNO-EXPERIENCES

We have seen that lack of exact material data makes it difficult to model the penetration experiments against steel and ceramics+backing. It could be interesting to see how this problem is handled by other research groups working in this field.

In a presentation (15) on the annual ANNC WGIII-meeting 2004, Martin van der Voorde from TNO described numerical simulations very similar to the ones performed in this report. Problems were pointed out, in particular, regarding simulations of a 14.5 mm API B-32 against ceramics and titanium respectively. It was found that using the same projectile properties, it was impossible to achieve correct results both for penetration into ceramic and titanium. Further, a literature survey had been carried out which seemed to reveal that this was a very common problem, which was usually fixed by "tuning" some parameters from the Autodyn material library to make the simulation fit the experimental results.

TNO proposed a collaborative program for dynamic and static material characterization to improve the knowledge of the projectile material properties.

10 CONCLUSION

We have tried to perform numerical simulations to compare with the experimental results given in (2). A major problem was that accurate material models for neither the projectile nor the various targets were available. Using a conversion method from Vicker's hardness to yield strength we were able to get reasonable good results in some cases. However, it was seen to be impossible to achieve complete consistency using these material parameters. By tinkering with the various materials parameters for the projectile, we would surely be able to achieve such a consistency, but this is a not a good solution since it does not help us dealing with

different target materials in the future. Our goal must be to obtain results from numerical simulations that give us information about the outcome of a penetration experiment, not to tune parameters in a simulation to obtain consistency with an already performed experiment. Before proceeding with simulations of more complex target configurations and exotic materials, it would surely be worthwhile to devote some effort to establishing proper material data for the projectile.

It was seen that other research groups were having the similar problems.

References

- (1) Fykse H, Private conversation
- (2) Horsfall I, Ehsan N, Bishop W, A comparison of the performance of various light armour piercing ammunition, Journal of Battlefield Technology, Vol 3, No 3, November 2000
- (3) Autodyn Theory Manual, Century Dynamics Ltd.
- (4) Moxnes J F, Private conversation
- (5) http://www.gordonengland.co.uk/hardness/brinell_conversion_chart.htm
- (6) Dullum O, Fykse H, Private conversation
- (7) Friis E K, Moxnes J F, Penetration of tungsten carbide into steel targets, Proceedings of the 21st Int Symposium on Ballistics, Adelaide, Australia, April 2004
- (8) Børvik T, Langseth M, Jenssen A, Langberg H, Smedsrød Ø, Use of aluminium panels as lightweight ballistic protection, Proceedings of the Norway-Singapore Workshop on Protection, Oslo, 3-5 november 2003
- (9) Autodyn material library, Century Dynamics Ltd.
- (10) Hiermaier, Riedel, Hayhurst, Clegg, Wentzel - "Advanced Material Models for HVI Simulations" - EMI Report No. E43/99, ESA CR(P) 4305, 1999
- (11) Sjøhl H, Teland J A, Perforation of concrete targets, FFI/RAPPORT-2001/05786
- (12) Teland J A, Multifunctional Numerical Tool for Penetration Analysis, FFI/NOTAT-2002/04647
- (13) Teland J A, Moxnes John F, Analytical cavity expansion penetration models compared with numerical simulations, Proceedings of the 11th Int. symposium on the interactions of the effects of munitions with structures, Mannheim mai 2003
- (14) Olsen Å A F, Teland J A, Rapid Autodyn-3D penetration simulations using a virtual target, FFI/RAPPORT-2002/00575
- (15) van der Voorde M, Ceramic protection, Minutes of the 2004 annual meeting of ANNC WGIII, FFI/RAPPORT-2004/03687

A CONVERSION CHART FOR VICKER'S HARDNESS TO YIELD STRENGTH

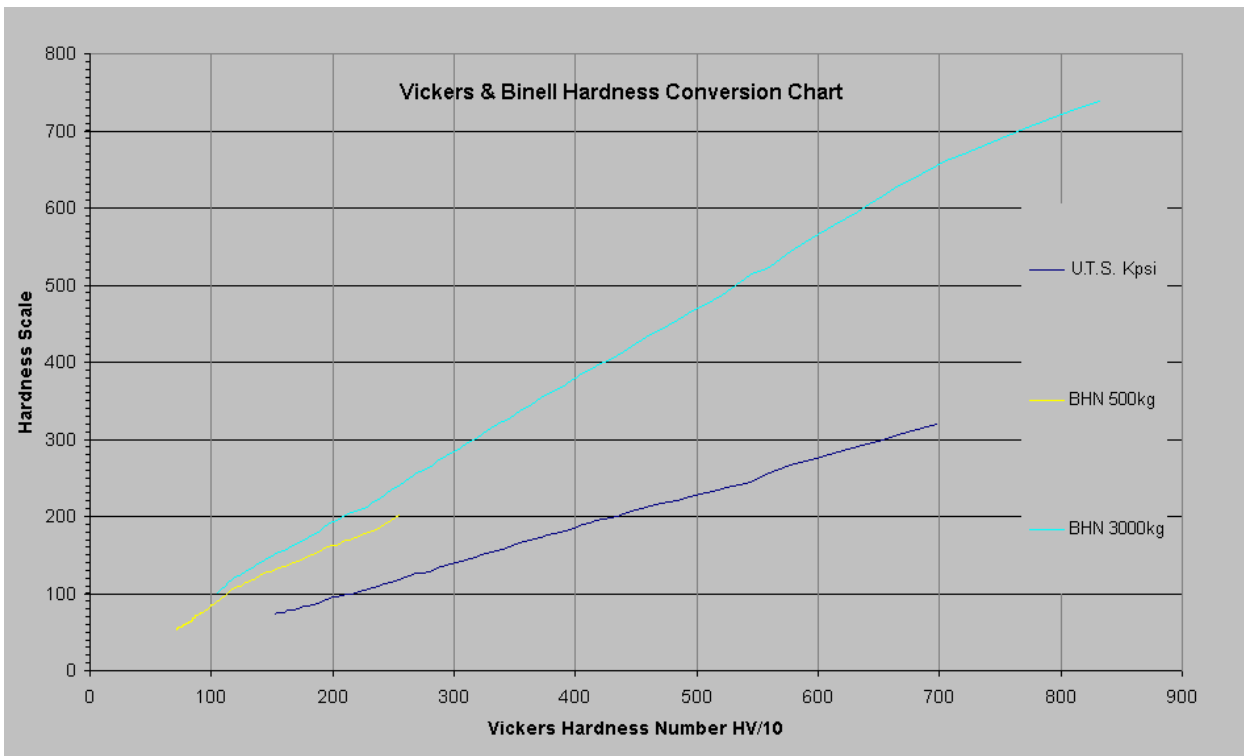


Figure A.1: Chart which gives relationship between Vicker's Hardness, Brinell Hardness and Ultimate Tensile strength

B MATERIAL MODELS

Tungsten Carbide

Equation of State	Compaction
Reference density	1.45500E+01
Density #1	1.45500E+01 (g/cm ³)
Density #2	1.70000E+01 (g/cm ³)
Density #3	0.00000E+00 (g/cm ³)
Density #4	0.00000E+00 (g/cm ³)
Density #5	0.00000E+00 (g/cm ³)
Density #6	0.00000E+00 (g/cm ³)
Density #7	0.00000E+00 (g/cm ³)
Density #8	0.00000E+00 (g/cm ³)
Density #9	0.00000E+00 (g/cm ³)
Density #10	0.00000E+00 (g/cm ³)

Pressure #1	0.00000E+00 (kPa)
Pressure #2	5.81000E+07 (kPa)
Pressure #3	0.00000E+00 (kPa)
Pressure #4	0.00000E+00 (kPa)
Pressure #5	0.00000E+00 (kPa)
Pressure #6	0.00000E+00 (kPa)
Pressure #7	0.00000E+00 (kPa)
Pressure #8	0.00000E+00 (kPa)
Pressure #9	0.00000E+00 (kPa)
Pressure #10	0.00000E+00 (kPa)
Density (Soundspeed) #1	1.45500E+01 (g/cm3)
Density (Soundspeed) #2	1.70000E+01 (g/cm3)
Density (Soundspeed) #3	0.00000E+00 (g/cm3)
Density (Soundspeed) #4	0.00000E+00 (g/cm3)
Density (Soundspeed) #5	0.00000E+00 (g/cm3)
Density (Soundspeed) #6	0.00000E+00 (g/cm3)
Density (Soundspeed) #7	0.00000E+00 (g/cm3)
Density (Soundspeed) #8	0.00000E+00 (g/cm3)
Density (Soundspeed) #9	0.00000E+00 (g/cm3)
Density (Soundspeed) #10	0.00000E+00 (g/cm3)
Soundspeed #1	4.86900E+03 (m/s)
Soundspeed #2	4.50500E+03 (m/s)
Soundspeed #3	0.00000E+00 (m/s)
Soundspeed #4	0.00000E+00 (m/s)
Soundspeed #5	0.00000E+00 (m/s)
Soundspeed #6	0.00000E+00 (m/s)
Soundspeed #7	0.00000E+00 (m/s)
Soundspeed #8	0.00000E+00 (m/s)
Soundspeed #9	0.00000E+00 (m/s)
Soundspeed #10	0.00000E+00 (m/s)
Strength	MO Granular
Pressure #1	-3.00000E+06 (kPa)

Pressure #2	-9.00000E+05 (kPa)
Pressure #3	1.80000E+06 (kPa)
Pressure #4	4.98000E+07 (kPa)
Pressure #5	0.00000E+00 (kPa)
Pressure #6	0.00000E+00 (kPa)
Pressure #7	0.00000E+00 (kPa)
Pressure #8	0.00000E+00 (kPa)
Pressure #9	0.00000E+00 (kPa)
Pressure #10	0.00000E+00 (kPa)
Yield Stress (zero plastic strain)	0.00000E+00 (kPa)
Yield Stress #2	2.75000E+06 (kPa)
Yield Stress #3	5.50000E+06 (kPa)
Yield Stress #4	6.15000E+07 (kPa)
Yield Stress #5	0.00000E+00 (kPa)
Yield Stress #6	0.00000E+00 (kPa)
Yield Stress #7	0.00000E+00 (kPa)
Yield Stress #8	0.00000E+00 (kPa)
Yield Stress #9	0.00000E+00 (kPa)
Yield Stress #10	0.00000E+00 (kPa)
Density #1	1.30000E+01 (g/cm3)
Density #2	1.50000E+01 (g/cm3)
Density #3	1.60000E+01 (g/cm3)
Density #4	1.70000E+01 (g/cm3)
Density #5	1.80000E+01 (g/cm3)
Density #6	1.90000E+01 (g/cm3)
Density #7	2.00000E+01 (g/cm3)
Density #8	2.10000E+01 (g/cm3)
Density #9	2.20000E+01 (g/cm3)
Density #10	2.30000E+01 (g/cm3)
Yield Stress (zero plastic strain)	3.66700E+06 (kPa)
Yield Stress #2	3.66700E+06 (kPa)
Yield Stress #3	3.66700E+06 (kPa)

Yield Stress #4	3.66700E+06 (kPa)
Yield Stress #5	3.66700E+06 (kPa)
Yield Stress #6	3.66700E+06 (kPa)
Yield Stress #7	3.66700E+06 (kPa)
Yield Stress #8	3.66700E+06 (kPa)
Yield Stress #9	3.66700E+06 (kPa)
Yield Stress #10	3.66700E+06 (kPa)
Density #1	1.30000E+01 (g/cm3)
Density #2	1.50000E+01 (g/cm3)
Density #3	1.60000E+01 (g/cm3)
Density #4	1.70000E+01 (g/cm3)
Density #5	1.80000E+01 (g/cm3)
Density #6	1.90000E+01 (g/cm3)
Density #7	2.00000E+01 (g/cm3)
Density #8	2.10000E+01 (g/cm3)
Density #9	2.20000E+01 (g/cm3)
Density #10	2.30000E+01 (g/cm3)
Shear Modulus #1	1.52900E+08 (kPa)
Shear Modulus #2	1.52900E+08 (kPa)
Shear Modulus #3	1.52900E+08 (kPa)
Shear Modulus #4	1.52900E+08 (kPa)
Shear Modulus #5	1.52900E+08 (kPa)
Shear Modulus #6	1.52900E+08 (kPa)
Shear Modulus #7	1.52900E+08 (kPa)
Shear Modulus #8	1.52900E+08 (kPa)
Shear Modulus #9	1.52900E+08 (kPa)
Shear Modulus #10	1.52900E+08 (kPa)
Failure	User failure #1
FC(1)	0.00000E+00 (kPa)
FC(2)	0.00000E+00 (kPa)
FC(3)	0.00000E+00 (kPa)
FC(4)	0.00000E+00 (kPa)

FC(5)	0.00000E+00 (kPa)
FC(6)	0.00000E+00 (kPa)
FC(7)	0.00000E+00 (kPa)
FC(8)	0.00000E+00 (kPa)
FC(9)	0.00000E+00 (kPa)
FC(10)	0.00000E+00 (kPa)
Erosion	None
Material Cutoffs	-
Maximum Expansion	1.00000E-01 (none)
Minimum Density Factor (Euler)	1.00000E-05 (none)
Minimum Density Factor (SPH)	2.00000E-01 (none)
Maximum Density Factor (SPH)	3.00000E+00 (none)
Minimum Soundspeed	1.00000E-06 (m/s)
Maximum Soundspeed	1.01000E+20 (m/s)
Maximum Temperature	1.01000E+20 (m/s)

Mild target steel

Equation of State	Linear
Reference density	7.83000E+00
Bulk Modulus	1.59000E+08 (kPa)
Reference Temperature	3.00000E+02 (K)
Specific Heat	4.77000E+02 (J/kgK)
Thermal Conductivity	0.00000E+00 (J/mKs)
Strength	Johnson Cook
Shear Modulus	8.18000E+07 (kPa)
Yield Stress	2.90000E+05 (kPa)
Hardening Constant	5.10000E+05 (kPa)
Hardening Exponent	2.60000E-01 (none)
Strain Rate Constant	1.40000E-02 (none)
Thermal Softening Exponent	1.03000E+00 (none)
Melting Temperature	1.79300E+03 (K)
Strain Rate Correction	1st Order

Failure	None
Erosion	Geometric Strain
Erosion Strain	4.00000E+00 (none)
Type of Geometric Strain	Instantaneous
Material Cutoffs	-
Maximum Expansion	1.00000E-01 (none)
Minimum Density Factor (Euler)	1.00000E-05 (none)
Minimum Density Factor (SPH)	2.00000E-01 (none)
Maximum Density Factor (SPH)	3.00000E+00 (none)
Minimum Soundspeed	1.00000E-06 (m/s)
Maximum Soundspeed	1.01000E+20 (m/s)
Maximum Temperature	1.01000E+20 (m/s)
Reference:	-

Hard target steel

Equation of State	Linear
Reference density	7.83000E+00
Bulk Modulus	1.59000E+08 (kPa)
Reference Temperature	3.00000E+02 (K)
Specific Heat	4.77000E+02 (J/kgK)
Thermal Conductivity	0.00000E+00 (J/mKs)
Strength	Johnson Cook
Shear Modulus	8.18000E+07 (kPa)
Yield Stress	1.14300E+06 (kPa)
Hardening Constant	5.10000E+05 (kPa)
Hardening Exponent	2.60000E-01 (none)
Strain Rate Constant	1.40000E-02 (none)
Thermal Softening Exponent	1.03000E+00 (none)
Melting Temperature	1.79300E+03 (K)
Strain Rate Correction	1st Order
Failure	None

Erosion	Geometric Strain
Erosion Strain	4.00000E+00 (none)
Type of Geometric Strain	Instantaneous
Material Cutoffs	-
Maximum Expansion	1.00000E-01 (none)
Minimum Density Factor (Euler)	1.00000E-05 (none)
Minimum Density Factor (SPH)	2.00000E-01 (none)
Maximum Density Factor (SPH)	3.00000E+00 (none)
Minimum Soundspeed	1.00000E-06 (m/s)
Maximum Soundspeed	1.01000E+20 (m/s)
Maximum Temperature	1.01000E+20 (m/s)

Aluminium

Equation of State	Linear
Reference density	2.66000E+00
Bulk Modulus	6.86200E+07 (kPa)
Reference Temperature	0.00000E+00 (K)
Specific Heat	0.00000E+00 (J/kgK)
Thermal Conductivity	0.00000E+00 (J/mKs)
Strength	Johnson Cook
Shear Modulus	2.63320E+07 (kPa)
Yield Stress	1.67000E+05 (kPa)
Hardening Constant	5.96000E+05 (kPa)
Hardening Exponent	5.51000E-01 (none)
Strain Rate Constant	1.00000E-03 (none)
Thermal Softening Exponent	8.59000E-01 (none)
Melting Temperature	8.93000E+02 (K)
Strain Rate Correction	1st Order
Failure	Hydro (Pmin)
Hydro Tensile Limit	-2.75000E+05 (kPa)
Reheal	Yes
Crack Softening	No

Stochastic failure	No
Erosion	Geometric Strain
Erosion Strain	4.00000E+00 (none)
Type of Geometric Strain	Instantaneous

Projectile Steel

Equation of State	Linear
Reference density	7.83000E+00
Bulk Modulus	1.59000E+08 (kPa)
Reference Temperature	3.00000E+02 (K)
Specific Heat	4.77000E+02 (J/kgK)
Thermal Conductivity	0.00000E+00 (J/mKs)
Strength	Johnson Cook
Shear Modulus	8.18000E+07 (kPa)
Yield Stress	1.00000E+06 (kPa)
Hardening Constant	5.10000E+05 (kPa)
Hardening Exponent	2.60000E-01 (none)
Strain Rate Constant	1.40000E-02 (none)
Thermal Softening Exponent	1.03000E+00 (none)
Melting Temperature	1.79300E+03 (K)
Strain Rate Correction	1st Order
Failure	None
Erosion	Geometric Strain
Erosion Strain	4.00000E+00 (none)
Type of Geometric Strain	Instantaneous

Brass

Equation of State	Shock
Reference density	8.45000E+00
Gruneisen coefficient	2.04000E+00 (none)
Parameter C1	3.72600E+03 (m/s)

Parameter S1	1.43400E+00 (none)
Parameter Quad. S2	0.00000E+00 (s/m)
Relative volume, VE	0.00000E+00 (none)
Relative volume, VB	0.00000E+00 (none)
Parameter C2	0.00000E+00 (m/s)
Parameter S2	0.00000E+00 (none)
Reference Temperature	0.00000E+00 (K)
Specific Heat	0.00000E+00 (J/kgK)
Thermal Conductivity	0.00000E+00 (J/mKs)
Strength	von Mises
Shear Modulus	3.00000E+07 (kPa)
Yield Stress	6.90000E+04 (kPa)
Failure	None
Erosion	Geometric Strain
Erosion Strain	2.00000E+00 (none)
Type of Geometric Strain	Instantaneous

Lead

Equation of State	Shock
Reference density	1.13500E+01
Gruneisen coefficient	2.77000E+00 (none)
Parameter C1	2.05100E+03 (m/s)
Parameter S1	1.46000E+00 (none)
Parameter Quad. S2	0.00000E+00 (s/m)
Relative volume, VE	0.00000E+00 (none)
Relative volume, VB	0.00000E+00 (none)
Parameter C2	0.00000E+00 (m/s)
Parameter S2	0.00000E+00 (none)
Reference Temperature	0.00000E+00 (K)
Specific Heat	0.00000E+00 (J/kgK)
Thermal Conductivity	0.00000E+00 (J/mKs)

Strength	von Mises
Shear Modulus	4.00000E+06 (kPa)
Yield Stress	5.00000E+03 (kPa)
Failure	None
Erosion	Geometric Strain
Erosion Strain	2.00000E+00 (none)
Type of Geometric Strain	Instantaneous

Copper

Equation of State	Linear
Reference density	8.96000E+00
Bulk Modulus	1.29000E+08 (kPa)
Reference Temperature	3.00000E+02 (K)
Specific Heat	3.83000E+02 (J/kgK)
Thermal Conductivity	0.00000E+00 (J/mKs)
Strength	Johnson Cook
Shear Modulus	4.60000E+07 (kPa)
Yield Stress	9.00000E+04 (kPa)
Hardening Constant	2.92000E+05 (kPa)
Hardening Exponent	3.10000E-01 (none)
Strain Rate Constant	2.50000E-02 (none)
Thermal Softening Exponent	1.09000E+00 (none)
Melting Temperature	1.35600E+03 (K)
Strain Rate Correction	1st Order
Failure	None
Erosion	Geometric Strain
Erosion Strain	3.00000E+00 (none)
Type of Geometric Strain	Instantaneous

Alumina

Equation of State	Polynomial
Reference density	3.89000E+00
Bulk Modulus A1	2.31000E+08 (kPa)
Parameter A2	-1.60000E+08 (kPa)
Parameter A3	2.77400E+09 (kPa)
Parameter B0	0.00000E+00 (none)
Parameter B1	0.00000E+00 (none)
Parameter T1	2.31000E+08 (kPa)
Parameter T2	0.00000E+00 (kPa)
Reference Temperature	0.00000E+00 (K)
Specific Heat	0.00000E+00 (J/kgK)
Thermal Conductivity	0.00000E+00 (J/mKs)
Strength	Johnson-Holmquist
Shear Modulus	1.52000E+08 (kPa)
Model Type	Continuous (JH2)
Hugoniot Elastic Limit	6.57000E+06 (kPa)
Intact Strength Constant A	8.80000E-01 (none)
Intact Strength Exponent N	6.40000E-01 (none)
Strain Rate Constant C	7.00000E-03 (none)
Fractured Strength Constant B	2.80000E-01 (none)
Fractured Strength Exponent M	6.00000E-01 (none)
Max. Fracture Strength Ratio	1.00000E+00 (none)
Failure	Johnson Holmquist
Hydro Tensile Limit	-2.62000E+05 (kPa)
Model Type	Continuous (JH2)
Damage Constant, D1	1.00000E-02 (none)
Damage Constant, D2	7.00000E-01 (none)
Bulking Constant, Beta	1.00000E+00 (none)
Damage Type	Gradual (JH2)
Tensile Failure	Hydro (Pmin)
Erosion	Geometric Strain

Erosion Strain	2.00000E+00 (none)
Type of Geometric Strain	Instantaneous

Kevlar-Epoxy

Equation of State	Ortho
Reference density	1.65000E+00
Stiffness	Stiffness Matrix
C11	3.42500E+06 (kPa)
C22	1.35000E+07 (kPa)
C33	1.35000E+07 (kPa)
C12	1.14000E+06 (kPa)
C23	1.20000E+06 (kPa)
C31	1.14000E+06 (kPa)
Shear Modulus 12	1.00000E+06 (kPa)
Shear Modulus 23	1.00000E+06 (kPa)
Shear Modulus 31	1.00000E+06 (kPa)
Material axes	X-Y-Z Space
Rotation angle about 11 (degrees)	0.00000E+00 (none)
X-coord. for dirn 11 (XYZ)	0.00000E+00 (mm)
Y-coord. for dirn 11 (XYZ)	0.00000E+00 (mm)
Z-coord. for dirn 11 (XYZ)	1.00000E+00 (mm)
Volumetric response	Polynomial
Bulk Modulus A1	4.15389E+06 (kPa)
Parameter A2	4.00000E+07 (kPa)
Parameter A3	0.00000E+00 (kPa)
Parameter B0	0.00000E+00 (none)
Parameter B1	0.00000E+00 (none)
Parameter T1	4.15389E+06 (kPa)
Parameter T2	0.00000E+00 (kPa)
Reference Temperature	3.00000E+02 (K)
Specific Heat	1.42000E+03 (J/kgK)

Thermal Conductivity	0.00000E+00 (J/mKs)
Strength	Elastic
Shear Modulus	1.00000E+06 (kPa)
Failure	Material Stress/Strain
Tensile Failure Stress 11	1.00000E+20 (kPa)
Tensile Failure Stress 22	1.00000E+20 (kPa)
Tensile Failure Stress 33	1.00000E+20 (kPa)
Maximum Shear Stress 12	1.00000E+20 (kPa)
Maximum Shear Stress 23	1.01000E+20 (kPa)
Maximum Shear Stress 31	1.01000E+20 (kPa)
Tensile Failure Strain 11	1.00000E-02 (none)
Tensile Failure Strain 22	8.00000E-02 (none)
Tensile Failure Strain 33	8.00000E-02 (none)
Maximum Shear Strain 12	1.00000E+20 (none)
Maximum Shear Strain 23	1.01000E+20 (none)
Maximum Shear Strain 31	1.01000E+20 (none)
Material Axes Option	IJK Space
Rotation angle about 11 (degrees)	0.00000E+00 (none)
Post Failure Option	Orthotropic
Residual Shear Stiffness Fraction	2.00000E-01 (none)
Maximum Residual Shear Stress	1.00000E+20 (kPa)
Decomposition Temperature	7.00000E+02 (K)
Matrix Melt Temperature	1.01000E+20 (K)
Failed in 11, Failure Mode	11 only
Failed in 22, Failure Mode	22 only
Failed in 33, Failure Mode	33 only
Failed in 12, Failure Mode	12 & 11 only
Failed in 23, Failure Mode	23 & 11 only
Failed in 31, Failure Mode	31 & 11 only
Melt Matrix Failure Mode	Bulk
Stochastic failure	No
Erosion	Geometric Strain

Erosion Strain	2.50000E+00 (none)
Type of Geometric Strain	Instantaneous
Material Cutoffs	-